ChemPubSoc Europe

DOI: 10.1002/chem.201600657

CHEMISTRY
A European Journal
Full Paper

Neoglycopeptides

Mechanistic Insight into Nanomolar Binding of Multivalent Neoglycopeptides to Wheat Germ Agglutinin

Philipp Rohse and Valentin Wittmann*[a]

Abstract: Multivalent carbohydrate–protein interactions are frequently involved in essential biological recognition processes. Accordingly, multivalency is often also exploited for the design of high-affinity lectin ligands aimed at the inhibition of such processes. In a previous study (D. Schwefel et al., *J. Am. Chem. Soc.* **2010**, *132*, 8704–8719) we identified a tetravalent cyclopeptide-based ligand with nanomolar affinity to the model lectin wheat germ agglutinin (WGA). To unravel the structural features of this ligand required for high-affinity binding to WGA, we synthesized a series of cyclic and linear neoglycopeptides that differ in their conformational freedom as well as the number of GlcNAc residues. Combined evidence from isothermal titration calorimetry (ITC), enzyme-linked lectin assays (ELLA), and dynamic light scattering (DLS) revealed different binding modes of tetra- and divalent ligands and that conformational preorganization of the ligands by cyclization is not a prerequisite for achieving high binding affinities. The high affinities of the tetravalent ligands rather stem from their ability to form crosslinks between several WGA molecules. The results illustrate that binding affinities and mechanisms are strongly dependent on the used multivalent system which offers opportunities to tune and control binding processes.

Introduction

Multivalency is a key concept of many biological recognition processes.[1] It enables strong binding using multiple weak individual interactions,[2] and it is of special importance in the field of carbohydrate–lectin interactions.[3] Lectins are carbohydrate-binding proteins that mostly exist as oligomers exhibiting multiple binding sites.[4] Multivalent carbohydrate ligands can have remarkably enhanced binding affinities over monovalent ligands, an observation referred to as the glycoside cluster effect.[5] In addition, multivalency not only results in increased binding affinity but often also in increased specificity. In the past, many different scaffolds have been designed and decorated with carbohydrates resulting in multivalent ligands with varying geometry.[6] Studies with these compounds have shown that the design of a multivalent ligand is decisive for its potency, and frequently it is observed that even small changes of the structure of ligands result in drastically altered binding affinities.[7] The binding enhancements are often attributed to the ability of a multivalent ligand to bridge adjacent binding sites (chelate effect),[8] although structural data that prove chelating binding are available in only a few cases.[9] Other explanations that are discussed but less well understood include crosslinking and statistical rebinding.[10] In this respect it is worth mentioning that multivalent inhibitors of glycosidases also show strongly increased activity although these enzymes usually have only a single active site.[11] To find optimal geometries of multivalent ligands in cases where structural or mechanistic data are missing, combinatorial approaches have been developed that allow for screening of large libraries of spatially diverse glycoclusters.[12] For a rational design of multivalent ligands with desired properties, however, an understanding of the underlying principles leading to binding enhancement is crucial.

Wheat germ agglutinin (WGA) is a plant lectin found in *Triticum vulgaris* that served as a model lectin in numerous studies with multivalent ligands. At neutral pH the protein forms a stable homodimer.[13] Eight binding sites have been identified at the interface of the two monomers.[13a,14] Four of them are termed primary binding sites due to their enhanced affinity to the natural ligand *N*-acetylglucosamine (GlcNAc). Binding to the remaining sites, which are called secondary binding sites, has been reported to be too weak to be detected in solution. In the past many different multivalent ligands for WGA have been developed. Those included glycopolymers,[15] dendrimers,[16] cyclodextrins,[17] quantum dots,[18] calixarenes,[19] di- to tetravalent glycoclusters,[7a,20] and octasilsesquioxanes.[21]

Previously, we employed cyclic peptides as scaffolds to generate conformationally restricted glycoclusters.[12a] In a combinatorial approach we screened a library of almost 20000 spatially diverse neoglycopeptides for WGA ligands and identified a series of high-affinity ligands.[12b] Further optimization led to neoglycopeptide **1** (Figure 1A) with an exceptionally high affinity featuring carbamate linkages between the sugars and

[a] *P. Rohse, Prof. Dr. V. Wittmann*
Department of Chemistry and Konstanz Research School Chemical Biology (KoRS-CB)
University of Konstanz, 78457 Konstanz (Germany)
Fax: (+49) 7531-88-4573
E-mail: mail@valentin-wittmann.de

Supporting information for this article is available on the WWW under http://dx.doi.org/10.1002/chem.201600657.

© 2016 Wiley-VCH Verlag GmbH & Co. KGaA, Weinheim

These are not the final page numbers! ↗↗

the peptide.[22]According to isothermal titration calorimetry (ITC) measurements presented here (see below), **1** and a previously published tetravalent neoglycopeptide[7a] with nanomolar affinity are the best WGA ligands reported so far. To unravel the mechanism behind the high binding affinity, we solved a crystal structure of **1** in complex with WGA.[22] In this structure, only the substructure of **1** shaded grey in Figure 1 A was resolved whereas the remaining part of the glycopeptide resulted in diffuse electron density. The analysis revealed that the sugar residues at D-Dab^4 and D-Dab^5 bridge two adjacent binding sites. The conformation of this substructure resembled the dominant conformation of **1** in solution (determined by NMR spectroscopy), suggesting that the conformational preorganization of the cyclic peptide assisted divalent binding to WGA leading to the observed high affinity.[22] However, it could not be excluded that the two additional GlcNAc moieties attached to D-Dab^2 and D-Dab^7 also contribute to the high affinity of **1**.

Here we present a study aiming at a deeper understanding of the binding mechanism of **1** leading to its high affinity. We were especially interested in the importance of conformational preorganization of **1** and synthesized linear analogs with higher conformational freedom. Following the surprising result that the linear tetravalent compounds had the same high affinity as cyclic peptide **1**, we investigated the role of the two sugars at D-Dab^2 and D-Dab^7 that were not resolved in the crystal structure and synthesized a series of cyclic and linear *divalent* peptides with only two GlcNAc residues. Combined evidence from ITC, enzyme-linked lectin assays (ELLA), dynamic light scattering (DLS), and observation of precipitation in case of the tetravalent ligands led to the conclusion that it is not the preorganization of the ligands but rather their ability to form crosslinks between several WGA molecules that is responsible for the different measured binding affinities.

Results and Discussion

Design of Compounds

Figure 2 depicts the WGA ligands synthesized and investigated within this study. To examine the impact of the conformational preorganization of cyclic peptide **1** on binding affinity, we synthesized linear peptide **2**. In **2** the amino acids Lys^1 and Glu^8 that are involved in cyclization were replaced by alanine residues. To exclude any impact of the outer amino acids in positions 1, 8, and 9 on the conformation of the peptide, we also synthesized the shortened peptide **3**.

In order to study the relevance of the two sugar residues that were not resolved in the crystal structure of **1** with WGA, divalent neoglycopeptides **4**–**6** were designed which lack the GlcNAc residues at D-Dab^2 and D-Dab^7. To keep the overall conformational change as small as possible, we chose not to simply remove the GlcNAc residues but to replace them by mannose (Man) residues as it is known that mannose does not bind to WGA.[23] In the course of our investigations it became clear that more glycopeptide structures were necessary to complete the picture. Thus, the series **7**–**10** of neoglycopeptides was additionally synthesized.

Synthesis of Neoglycopeptides

The neoglycopeptides were prepared by employing Fmoc solid-phase peptide synthesis. α-Glycosyl *p*-nitrophenyl carbonates **11** and **14** (Scheme 1) served as precursors to generate carbamate-linked glycoamino acid building blocks by reaction with a suitable D-Dab derivative. The synthesis of GlcNAc carbonate **11** has been reported before.[22,24] To obtain the mannose carbonate **14**, peracetylated D-mannose **12** was selectively deprotected at the anomeric position using benzylamine yielding **13**[25] in 54% that—according to an NMR spectrum in $CDCl_3$—exists as pure α-anomer. Compound **13** was then reacted with *p*-nitrophenyl chloroformate to give carbonate **14** in a yield of 79% under retention of configuration. As shown in Scheme 2, carbonates **11** and **14** were then ligated to the side-chain amino group of Fmoc-D-Dab **15**. The glyco amino acids **16** and **17** were obtained in yields of 75% and 80%, respectively.

Solid-phase peptide synthesis was performed on TentaGel (in case of cyclic peptides) or polystyrene resins (in case of linear peptides) equipped with the Sieber linker.[26] Slightly different synthetic strategies were followed for the cyclic and linear peptides. This is shown in Scheme 3 exemplarily for

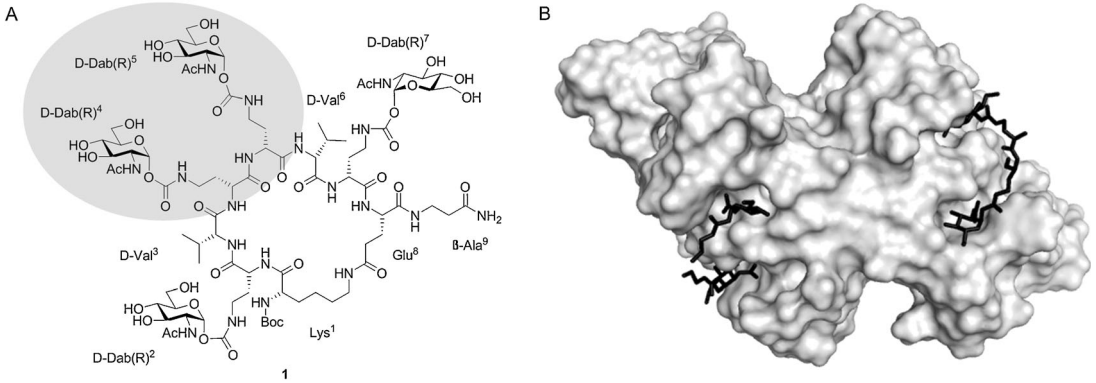

Figure 1. (A) Cyclic peptide **1** and (B) crystal structure of its complex with WGA (PDB ID: 2X3T). Only the grey shaded substructure of **1** is resolved in the crystal structure and shown as stick model (black). The WGA dimer is shown as surface representation (grey). D-Dab = D-diaminobutanoic acid.

© 2016 Wiley-VCH Verlag GmbH & Co. KGaA, Weinheim

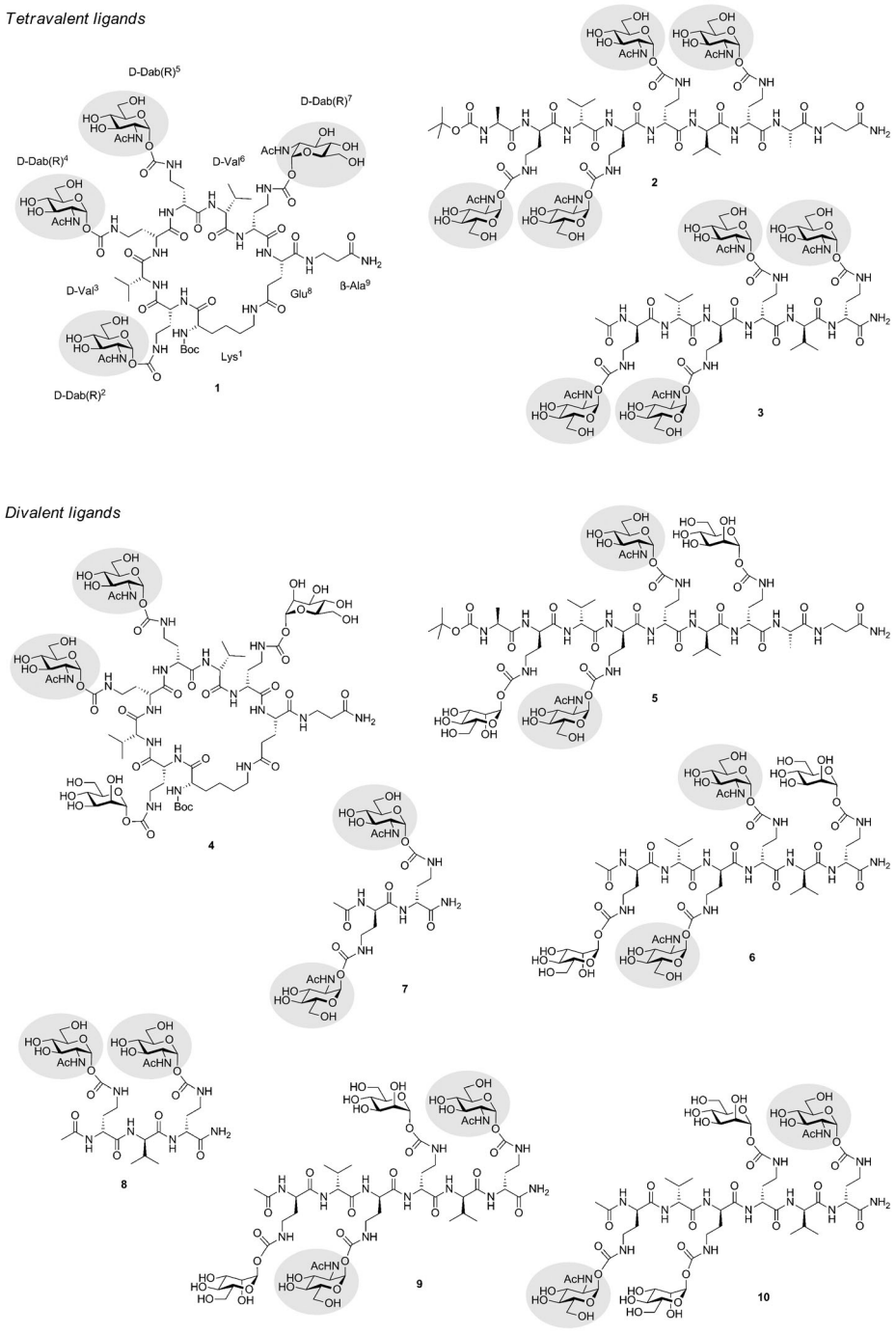

Figure 2. Tetravalent (**1**–**3**) and divalent glycopeptides (**4**–**10**) synthesized within this study. GlcNAc residues are shaded grey.

cyclic peptide **1** and linear peptide **2**. The other peptides depicted in Figure 2 were synthesized analogously. Starting from resin **18**, peptide assembly followed the Fmoc strategy using 2-(1*H*-benzotriazol-1-yl)-1,1,3,3-tetramethyluronium hexafluorophosphate (HBTU),[27] 1-hydroxybenzotriazole (HOBt), and Hünig's base (EtN*i*Pr$_2$) as coupling reagents (Scheme 3 A). Only in the last step, a Boc-protected amino acid was employed. Side-chain cyclization of peptide **19** was achieved on-resin after removal of the allyl-type protecting groups of lysine and glutamic acid with Pd(PPh$_3$)$_4$/BH$_3$•HNMe$_2$ by treatment with HOBt/HBTU/EtN*i*Pr$_2$ to yield **20** (Scheme 3 B). For a successful cyclization it was important to use a low resin loading to prevent crosslinking of the peptides on the resin.[22] This requirement is met by the commercially available TentaGel resin (typical loading: 0.2 mmol g^{-1}). The peptide was cleaved from the resin using 1% trifluoroacetic acid in CH_2Cl_2, and the carbohydrate residues were deacetylated with EtNMe$_2$/MeOH resulting in peptide **1**. The deprotection of the carbohydrate moieties was performed after cleavage from the resin to provide a better stability of the glycosidic linkages during acid cleav-

© 2016 Wiley-VCH Verlag GmbH & Co. KGaA, Weinheim

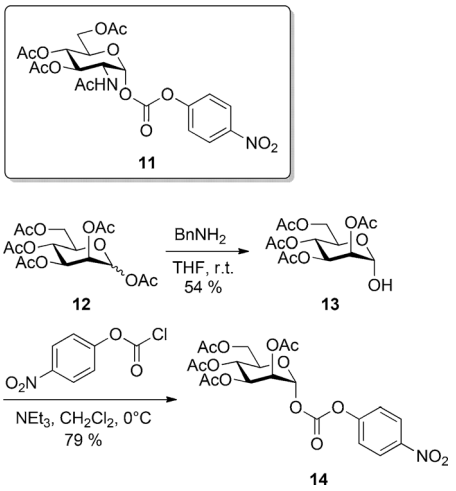

Scheme 1. Literature-known carbonate **11**[22,24] and synthesis of glycosyl carbonate **14**.

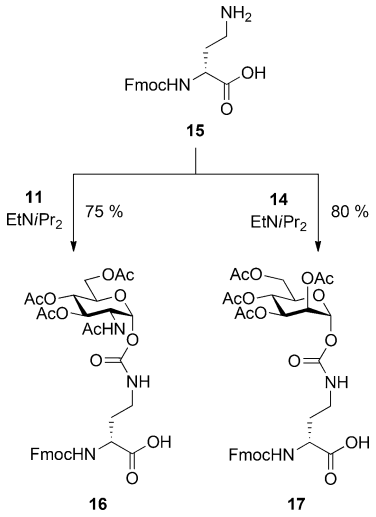

Scheme 2. Synthesis of carbamate-linked glycoamino acids **16** and **17**.

age from the resin.[12a] Linear peptide **2** with the same backbone length of nine amino acids was synthesized on polystyrene resin with the Sieber linker and a loading of 0.6 mmol g^{-1} (Scheme 3C). Lysine and glutamic acid that served for side-chain cyclization in case of peptide **1** were replaced by alanine. After peptide assembly, resin **21** was treated with 1% trifluoroacetic acid in CH_2Cl_2 to cleave the peptide from the resin. Subsequent deacetylation resulted in peptide **2**. All deacetylated peptides were finally purified by semi-preparative HPLC.

Influence of Conformational Preorganization of Tetravalent Ligands on Binding Affinity

We first investigated the importance of the conformational preorganization of tetravalent glycopeptide **1** for its high binding affinity. To this end we synthesized linear peptide **2** having the same amino acid sequence as **1** except for the amino acids used for cyclization which were replaced by alanine residues. Thermodynamic binding parameters were determined by ITC.

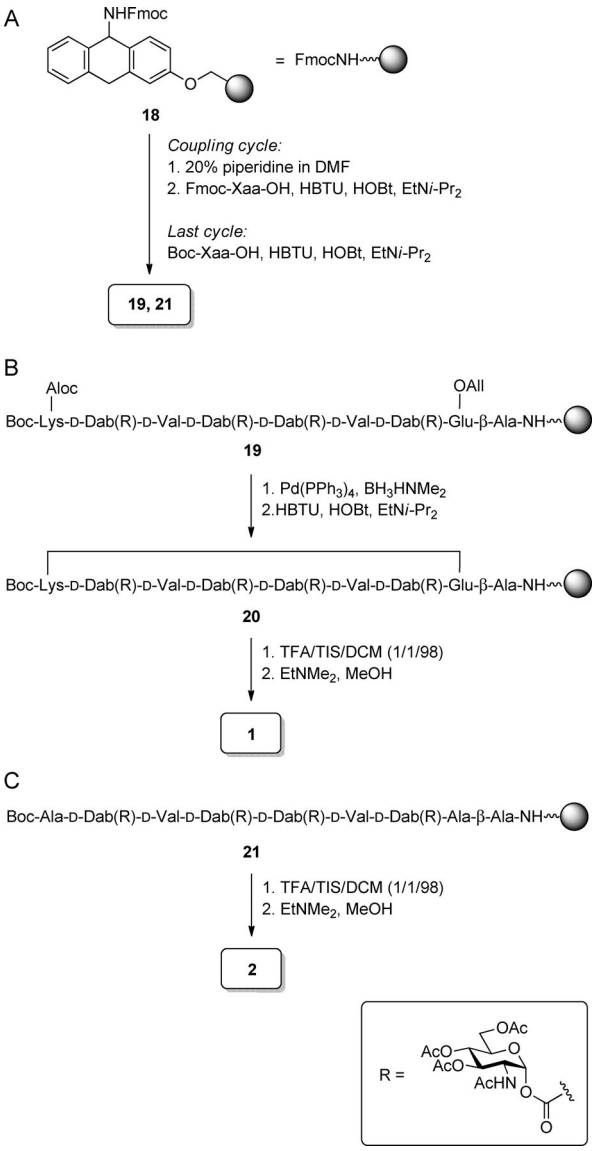

Scheme 3. Solid-phase peptide synthesisof cyclic peptide **1** and linear peptide **2**. (A) Synthesis of precursors **19** and **21**. (B) On-bead cyclization of **19** followed by cleavage from the resin and deacetylation gives **1**. (C) Treatment of **21** with cleavage cocktail followed by deacetylation gives **2**.

In contrast to enzyme-linked lectin assays, which deliver assay-dependent IC_{50} values, this technique gives access to K_d values including their enthalpic and entropic contributions and the stoichiometry of binding events without the need to label or immobilize ligand or protein. ITC has been proven to be well-suited to investigate carbohydrate-protein interactions.[28] Table 1 summarizes the results of the ITC measurements for all ligands (titration curves are shown in Figure S11–S20).

ITC experiments with the weak-binding monovalent GlcNAc were carried with a large excess of ligand and assuming a stoichiometry of 4 as recently suggested.[7a,29] With the tetravalent compounds we observed some precipitate formation as discussed below in more detail. In these cases the K_d values obtained by ITC thus are reported as "apparent K_d".

Cyclic peptide **1** shows a K_d value of 8.4 nM which is the same as that for the best WGA ligand reported so far.[7a] Inter-

© 2016 Wiley-VCH Verlag GmbH & Co. KGaA, Weinheim

Table 1. Thermodynamic binding parameters for tetravalent (**1**-**3**) and divalent neoglycopeptides (**4**–**10**) binding to WGA at pH 7.0 and 25 °C determined by ITC.[a]

Compound (valency)	K_d [μM]	n[b]	ΔH [kcal mol^{-1}]	$-T\Delta S$ [kcal mol^{-1}]	ΔG [kcal mol^{-1}]	β_{K_d}[d]
GlcNAc	1830 ± 81	4[c]	−7.06 ± 0.57	3.33 ± 0.61	−3.73 ± 0.03	1
1 (tetra)	0.0084 ± 0.0009	0.84 ± 0.03	−32.0 ± 0.08	21.0 ± 0.01	−11.0 ± 0.08	218 000
2 (tetra)	0.0070 ± 0.0003	0.95 ± 0.01	−38.5 ± 0.33	27.4 ± 0.36	−11.1 ± 0.03	261 000
3 (tetra)	0.0062 ± 0.0009	0.86 ± 0.03	−37.1 ± 2.06	25.9 ± 2.14	−11.2 ± 0.09	295 000
4 (di)	1.43 ± 0.04	1.81 ± 0.06	−16.0 ± 0.02	7.99 ± 0.01	−7.99 ± 0.02	1280
5 (di)	1.25 ± 0.04	1.82 ± 0.05	−15.0 ± 0.05	6.94 ± 0.06	−8.06 ± 0.01	1460
6 (di)	0.85 ± 0.25	2.01 ± 0.04	−17.4 ± 0.22	9.06 ± 0.18	−8.30 ± 0.04	2150
7 (di)	1.44 ± 0.03	1.48 ± 0.02	−16.4 ± 0.70	8.39 ± 0.70	−7.98 ± 0.01	1270
8 (di)	0.120 ± 0.002	1.59 ± 0.03	−19.6 ± 0.06	10.1 ± 0.07	−9.48 ± 0.13	15 250
9 (di)	0.151 ± 0.004	1.94 ± 0.07	−16.1 ± 0.16	6.76 ± 0.18	−9.30 ± 0.02	12 200
10 (di)	1.33 ± 0.1	1.75 ± 0.03	−15.4 ± 0.37	7.46 ± 0.46	−7.97 ± 0.09	1380

[a] Standard deviations were obtained from two independent experiments. [b] Stoichiometry of binding (ligands per WGA dimer). [c] Fixed during fit. [d] Relative binding affinities.

estingly, linear analog **2** which is lacking conformational restriction by cyclization has an even slightly better affinity of 7 nM. This suggests that conformational preorganization might not be an important factor for achieving high affinity. However, it cannot be excluded that it is the amino acid sequence that induces a preferred conformation of the peptide that is simply preserved during cyclization. Therefore, we shortened the sequence of the peptide as much as possible resulting in linear peptide **3** lacking all amino acids before the first and after the last sugar-modified D-Dab residue. Again, ITC measurements revealed no loss of binding affinity but a slightly smaller K_d value of 6.2 nM. Comparing the binding enthalpies and entropies of peptides **1**–**3**, the linear glycopeptides **2** and **3** have higher absolute values of the binding enthalpy ΔH but also higher absolute values of the binding entropy ΔS than the cyclic peptide. This is in line with the more flexible structure of the linear peptide which allows the individual carbohydrate epitopes to adapt better to the binding pocket, a process that, on the other hand, also results in a more pronounced loss of entropy compared to the cyclic peptide. In sum, this leads to a similar affinity of all tetravalent peptides investigated regardless of their cyclic or linear nature.

The tetravalent ligands were further investigated by an enzyme-linked lectin assay (ELLA). In the ELLA the ability of a ligand to inhibit the binding of a lectin to a surface coated with a reference ligand is evaluated. The ligand concentration at which half of the lectin binding to the surface is inhibited is defined as the IC_{50} value. Earlier, we developed an ELLA in which microtiter plates are covalently functionalized with GlcNAc residues.[20a] Here, we modified the assay by using a simpler tetra(ethylene glycol) linker to attach the carbohydrates to the surface. The dose-response curves for compounds **1**–**3** are shown in Figure 3, and the corresponding IC_{50} values are listed in Table 2. Also in the ELLA, all tetravalent ligands show high, comparable affinities. The IC_{50} value for peptide **1** is lower than the one reported before.[22] This demonstrates once again the strong dependence of IC_{50} values on the assay. Therefore, we used only ITC for our further investigations.

Relevance of the Sugars at Positions D-Dab^2 and D-Dab^7

Since the conformational restriction of cyclic peptide **1** turned out not to be an essential feature to arrive at high binding affinities in this case, we investigated the importance of the sugar residues in position D-Dab^2 and D-Dab^7 that were not resolved in the crystal structure of compound **1** (Figure 1B). We synthesized a series of divalent glycopeptides in which these sugars were replaced by mannose residues. Mannose is known to not be recognized by WGA. In this way we intended to keep the conformational properties of the peptides comparable to that of their tetravalent analogues.

The results of the ITC measurements are summarized in Table 1. Cyclic divalent peptide **4** showed a 170-fold lower binding affinity (K_d = 1.43 μM) compared to its tetravalent analogue **1**. This already emphasizes the importance of the two additional GlcNAc residues for the binding. Linear compounds **5** and **6** which are the divalent analogues of **2** and **3** also showed a considerably lower binding affinity with K_d values of 1.25 μM and 0.85 μM, respectively, comparable to cyclic divalent analogue **4**. Similarly, for compound **7**, which is the dipeptide substructure of peptide **4** comprising D-Dab^4 and D-Dab^5 residues visible in the crystal structure, a K_d value of 1.44 μM was determined.

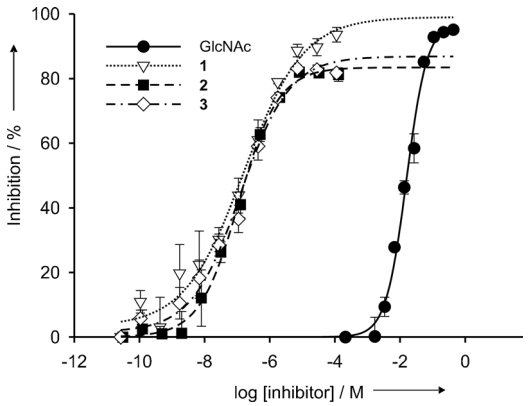

Figure 3. Dose-response curves for inhibition of the binding of HRP-labeled WGA to GlcNAc-coated microtiter plates by tetravalent glycopeptides **1**–**3**.

Table 2. Absolute and relative IC_{50} values of tetravalent glycopeptides **1**–**3** for inhibition of the binding of HRP-labeled WGA to covalently immobilized GlcNAc from dose-response curves shown in Figure 3.

Compound (valency)	IC_{50} [μM]	$\beta_{IC_{50}}$[a]
GlcNAc	15 700	1
1 (tetra)	0.112	140 000
2 (tetra)	0.126	125 000
3 (tetra)	0.161	98 000

[a] Relative inhibitory potency.

© 2016 Wiley-VCH Verlag GmbH & Co. KGaA, Weinheim

To complete the picture, we also synthesized divalent ligands **8**–**10**. Here, one GlcNAc residue was attached to D-Dab[7] whereas the second one was permuted between D-Dab[2], D-Dab[4], and D-Dab[5] resulting in increased distances between the GlcNAc residues compared to divalent ligands **4**–**7** in which the GlcNAc residues were attached to the adjacent amino acids D-Dab[4] and D-Dab[5]. In case of divalent ligands that are able to bridge adjacent binding sites, the binding affinity should be strongly dependent on the length of the linker unit between two carbohydrates. Indeed the binding affinity strongly increased for ligands **8** and **9** with K_d values of 0.12 μM and 0.15 μM, respectively, and decreased again to for ligand **10** ($K_d = 1.33$ μM) with the longest distance between the GlcNAc residues.

Beside the varied binding affinities we observed a striking difference between tetravalent and divalent peptides with respect to their WGA binding stoichiometry. Whereas the tetravalent ligands **1**–**3** show a binding of one ligand molecule per WGA dimer, the stoichiometry of the divalent peptides **4**–**10** is two ligands per WGA dimer (or somewhat lower) pointing to different binding modes. Remarkably, we also observed the formation of precipitates immediately upon titration of the tetravalent ligands into WGA solutions which was not the case with the divalent ligands. This, furthermore, emphasizes different binding modes between the two groups of ligands involving crosslinking in case of the tetravalent ligands. With values from 32 to 38.5 kcal mol^{-1}, the binding enthalpies ΔH of the tetravalent ligands are approx. twice the values of the divalent ligands (15–19.6 kcal mol^{-1}) indicating that all four GlcNAc residues are involved in WGA binding.

Dynamic Light Scattering Experiments

To further shed light on the binding modes of tetravalent and divalent ligands, we examined the kind of species present in WGA ligand mixtures. As mentioned above, precipitation was observed after ITC measurements of tetravalent ligands indicating the formation of big insoluble protein–ligand complexes. To further investigate the type of species remaining in solution, we performed DLS experiments. DLS is a method for the determination of the hydrodynamic radius of macromolecules or particles in solution. The neoglycopeptides were incubated for 1–3 h with WGA in a molar ratio of 1:1 for the tetravalent ligands **1**–**3** and 2:1 for the divalent ligands **4**–**10** according to the stoichiometries determined by ITC. Subsequently, the samples were filtered through a 100 nm cutoff filter to remove the formed precipitate and DLS measurements were performed with the filtrates. The results are shown in Figures 4 and 5 (see also Figure S21–S30). Similar results were obtained with a 1.2 μm cutoff filter (data not shown).

As shown in Figure 5 A, the species formed from WGA and tetravalent glycopeptides **1**–**3** are characterized by increased hydrodynamic radii in all cases. Whereas the WGA dimer alone has a hydrodynamic radius of 3.1 nm, r increases to 4.5–5.4 nm depending on the added ligand. This corresponds to an increase of the calculated molecular mass from 48 kDa for WGA to 120–177 kDa[30] after addition of a tetravalent ligand (Fig-

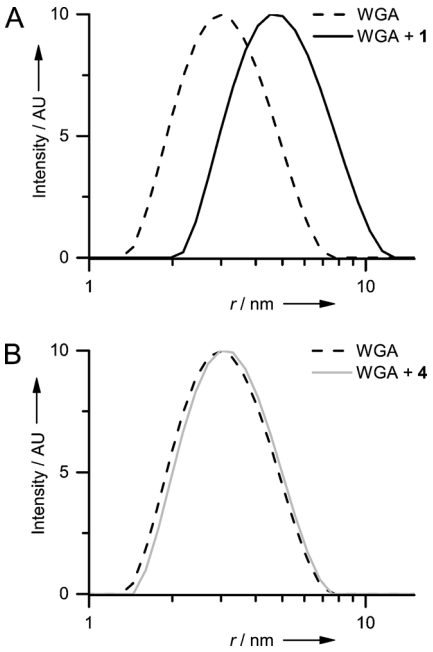

Figure 4. Typical intensity distributions of hydrodynamic radii r for tetravalent and divalent ligands exemplarily shown for mixtures of (A) tetravalent neoglycopeptide **1** and WGA dimer in a ratio of 1:1 (black curve) and (B) divalent cyclopeptide **4** and WGA dimer in a ratio of 2:1 (grey curve) in comparison to pure WGA (dashed curves) determined by DLS after filtration through a 100 nm cutoff filter.

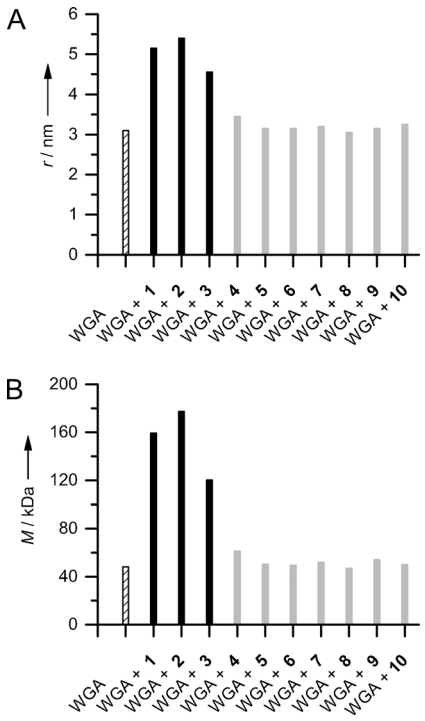

Figure 5. (A) Mean hydrodynamic radii r (derived from intensity distributions) of species present in solutions of WGA alone (hatched bars) and after addition of tetravalent (black bars) and divalent ligands (grey bars) determined by DLS after filtration through a 100 nm cutoff filter. (B) Molecular masses M of the species shown in A) calculated from the hydrodynamic radii by OmniSIZE 3.0 using the built-in protein model.

© 2016 Wiley-VCH Verlag GmbH & Co. KGaA, Weinheim

ure 5B). In case of the divalent ligands **4**–**10** on the other hand, no species with increased radii are detected, that is, no bigger aggregates are formed.

Discussion of Possible Binding Modes

According to the experimental results, one can propose different binding modes schematically shown in Figure 6. For the tetravalent ligands, the simplest explanation for the observed stoichiometry of ligand/WGA dimer of 1:1 would be a complex of one ligand bound to one WGA dimer bridging four binding sites (Figure 6A). However, this binding mode is not possible since the dimensions of the ligands do not allow a bridging of the four primary binding sites at the same time. In addition, the DLS measurements revealed that only bigger aggregates are found which can be explained by binding modes involving crosslinked species. Figure 6B depicts a theoretical binding mode in which two ligands interconnect two protein dimers. Modeling experiments, however, showed that also this binding mode is not possible as shown in Figure 6C. Considering the increase of molecular mass determined by DLS, aggregates with a stoichiometry of 3:3 seem most plausible (Figure 6D), and modeling experiments confirmed that three WGA dimers indeed can be arranged in a way that allows crosslinking by three ligands. Figure 6E and 6F illustrate oligomeric and polymeric binding modes with a net stoichiometry of 1:1 in which either higher-dimensional networks or one-dimensional chains are formed. Both can lead to large aggregates that eventually precipitate from the solution. Similar aggregate formation has been previously reported for bacterial toxins with dendrimer-based ligands of mismatched valency.[31]

For the divalent ligands the situation is different. In this case no precipitation could be detected and also DLS measurements showed that the hydrodynamic radii of WGA-ligand complexes were very similar to the radius of the protein alone. This result together with the ITC-derived stoichiometry of two ligands binding to one protein dimer indicates that no crosslinking occurs in case of the divalent ligands. Thus, only one binding mode is plausible. Both ligands bridge pairs of adjacent primary binding sites on one protein dimer. This binding mode is depicted in Figure 6G.

Conclusion

To dissect the structural features of tetravalent cyclopeptide **1** responsible for its high WGA binding affinity, we synthesized and investigated a series of tetra- and divalent neoglycopeptides derived from **1** that differ in their conformational freedom as well as the number of GlcNAc residues. Thermodynamic binding parameters were determined by ITC and revealed that the cyclic nature of **1** is not a prerequisite for high-affinity binding; linear tetravalent analogues of **1** showed a similar affinity which was also confirmed by ELLA experiments. Comparison of the tetravalent ligands with a series of cyclic and linear divalent ligands showed that all sugar residues of the tetravalent ligands are involved in protein binding and required to achieve low nanomolar affinity. The combination of DLS data, observed precipitation in case of the tetravalent ligands, and stoichiometries derived from ITC experiments allowed us to deduce different binding modes for the divalent and tetravalent ligands. The divalent ligands bind with a 2:1 stoichiometry in a chelating mode in which two ligand bridge two pairs of adjacent binding sites of a WGA dimer. In case of the tetravalent ligands, several binding modes are effective in parallel. Larger aggregates form and precipitate out. At the same time, small aggregates of a defined size, most probably with a stoichiometry of 3:3, remain in solution. In a more general view, the differences between the two series of ligands illustrate the strong dependence of binding affinities and mechanisms on the used multivalent system. Depending on the size and geometry of proteins and ligands, several binding modes may be possible and effective in parallel and in varying proportions. Multivalency which is common in nature enables not only high affinity interactions but the variation of scaffolds offers tremendous opportunities to tune binding affinities and control binding mechanisms.

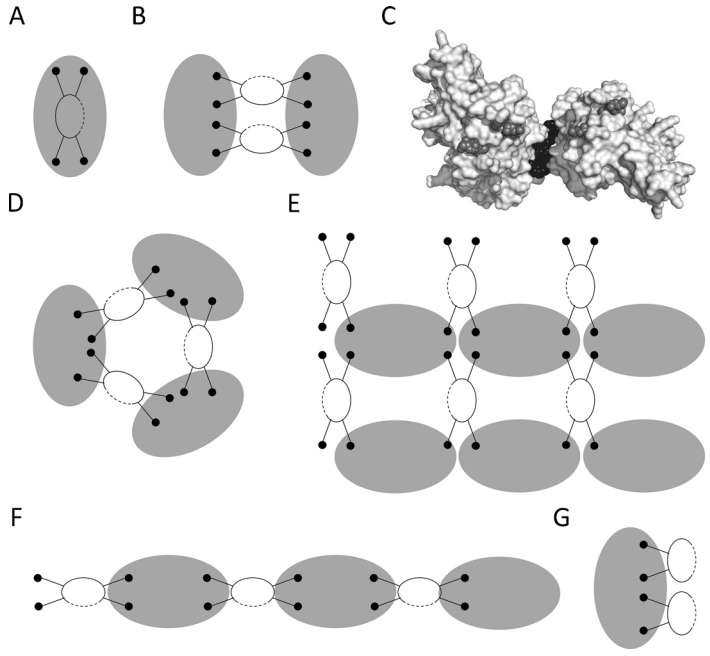

Figure 6. Schematic representation of conceivable binding modes of tetravalent (A–F) and divalent (G) ligands in complex with WGA that are in accordance with the determined binding stoichiometries. Cyclic or linear ligands are shown in black. Grey ellipses represent WGA dimers. (A) One tetravalent ligand bound to one WGA dimer in a 1:1 stoichiometry. (B) 2:2 stoichiometry. (C) Attempt to model a complex with 2:2 stoichiometry. Two WGA dimers are crosslinked by cyclic ligand **1** (black). It can be seen that a second molecule of **1** is not able to bridge the remaining primary binding sides (bound GlcNAc residues shown in medium grey) due to the convex surface of the protein (Figure created with PyMOL[32]). (D) 3:3 stoichiometry. (E), (F) Polymeric binding modes. (G) Binding mode of divalent ligands.

© 2016 Wiley-VCH Verlag GmbH & Co. KGaA, Weinheim

Experimental Section

General methods: Wheat germ agglutinin (lectin from *Triticum vulgaris*) was purchased from Sigma Aldrich. All reactions were monitored by TLC on silica gel 60 F254 (Merck) on aluminum sheets with detection by UV light ($\lambda = 254$ nm). Additionally, acidic ethanolic *p*-anisaldehyde solution followed by gentle heating was used for visualization. Preparative flash column chromatography (FC) was performed with an MPLC-Reveleris system from Grace. NMR spectra were recorded at room temperature on Avance III 400 and Avance III 600 instruments from Bruker. Chemical shifts are reported relative to solvent signals ($CDCl_3$: $\delta_H = 7.26$, $\delta_C = 77.16$; $[D_6]$DMSO: $\delta_H = 2.50$, $\delta_C = 39.52$). Signals were assigned by first-order analysis and, when feasible, assignments were supported by two-dimensional $^1H,^1H$ and $^1H,^{13}C$ correlation spectroscopy (COSY, HMBC and HSQC). High-resolution mass spectra (HRMS-ESI) were recorded on a Thermo LTQ Orbitrap Discovery with electrospray ionization. Semi-preparative high performance liquid chromatography (HPLC) was conducted on a LC-20A prominence system (pumps LC-20AT, auto sampler SIL-20A, column oven CTO-20AC, diode array detector SPD-M20A, ELSD-LT II detector, controller CBM-20 A and software LC-solution) from Shimadzu. A binary gradient of acetonitrile (with 0.1% formic acid or trifluoroacetic acid) (B) in water (with 0.1% formic acid or trifluoroacetic acid) (A) was used. For analytical HPLC a Nucleodur 100–5 C18 ec column from Macherey–Nagel (250×4 mm, flow 0.9 mL min^{-1}) was used. For semi-preparative HPLC a Eurosphere 100 C18 column from Knauer (16×250 nm, flow 8 mL min^{-1}), a Kinetex C18 column from Phenomenex (250×21.2 mm, flow 9 mL min^{-1}) and a Gemini C6-Phenyl column from Phenomenex (75×30 mm, flow 10 mL min^{-1}) were used. UV-Vis Absorption was measured using a Cary 50 instrument from Varian. Microtiter plates were read out with a FLUOstar OPTIMA plate reader from BMG Labtech.

2,3,4,6-Tetra-*O*-acetyl-1-*O*-*p*-nitrophenoxycarbonyl-α-D-mannopyranose (14): 2,3,4,6-Tetra-*O*-acetyl-D-mannopyranose (**13**)[25] (1.24 g, 3.56 mmol) and triethylamine (0.72 g, 7.1 mmol) were dissolved in dry CH_2Cl_2 (10 mL) in a Schlenk flask under nitrogen. *p*-Nitrophenyl chloroformate (1.57 g, 7.83 mmol) was dissolved in dry CH_2Cl_2 (10 mL) and added dropwise at 0 °C. The solution was stirred for 5.5 h and was allowed to warm up to room temperature. The solvent was evaporated and the residue was dissolved in EtOAc. The solution was washed with 5% (w/w) citric acid and water. The combined aqueous phases were re-extracted with EtOAc. The combined organic layers were dried with $MgSO_4$ and the solvent was evaporated. The crude material was purified by FC (silica, 16–100% EtOAc in petroleum ether over 13 min) to give **14** as a white solid (1.44 g, 79%). M.p. 136.6–137.5 °C; $R_f = 0.38$ (petroleum ether/EtOAc 1:1); ^1H NMR (400 MHz, $CDCl_3$): δ = 8.30 (d, J = 9.2 Hz, 2H; H^{Ar}), 7.43 (d, J = 9.3 Hz, 2H; H^{Ar}), 6.08 (d, J = 1.6 Hz, 1H; H-1), 5.43–5.41 (m, 3H; H-2, H-3, H-4), 4.35–4.31 (m, 1H; H-6a), 4.18–4.15 ppm (m, 2H; H-5, H-6b); ^{13}C NMR (101 MHz, $CDCl_3$): δ = 170.6 (O(*C*O)CH_3), 170.0 (O(*C*O)CH_3), 169.8 (O(*C*O)CH_3), 169.6 (O(*C*O)CH_3), 155.1 (O(*C*O)O), 150.3 (C^{Ar}), 145.9 (C^{Ar}), 125.6 (HC^{Ar}), 121.8 (HC^{Ar}), 95.2 (C-1), 71.4 (C-5), 68.5 (C-3), 68.0 (C-4), 65.4 (C-2), 62.0 (C-6), 20.9 (O(CO)*C*H_3), 20.8 (O(CO)*C*H_3), 20.77 (O(CO)*C*H_3), 20.7 ppm (O(CO)*C*H_3); elemental analysis calcd (%) for $C_{21}H_{23}NO_{14}$: C 49.13, H 4.52, N 2.73; found C 49.03, H 4.90, N 2.69.

(2*R*)-2-((9-Fluorenylmethoxycarbonyl)amino)-4-(((2-acetamido-3,4,6-tri-*O*-acetyl-2-deoxy-α-D-glucopyranosyl)-oxycarbonyl)amino)-butanoic acid (16): Fmoc-D-Dab-OH **15** (3 g, 8.81 mmol) was dissolved in dry DMF (150 mL) in a Schlenk flask under nitrogen. Diisopropyletylamine (3 mL, 17.6 mmol) was added and carbonate **11** (4.8 g, 9.9 mmol) was added as a solid. The solution was stirred at r.t. for 2 h. The solvent was evaporated and the crude was purified by FC (silica, MeCN/H_2O 10:1 to 5:1). Product **16** was obtained as a white amorphous solid (4.7 g, 75%). $R_f = 0.5$(MeCN:H_2O 3:1); ^1H NMR (400 MHz, $[D_6]$DMSO): δ = 8.06 (d, J = 8.4 Hz, 1H; N*H*(GlcNAc)), 7.88 (d, J = 7.4 Hz, 2H; H^{Ar}), 7.70 (d, J = 7.7 Hz, 2H; H^{Ar}), 7.53 (t, J = 4.9 Hz, 1H; NH^{γ}), 7.41 (t, J = 7.3 Hz, 2H; H^{Ar}), 7.32 (t, J = 7.1 Hz, 2H, H^{Ar}), 6.85 (d, J = 6.0 Hz, 1H; NH^{α}), 5.81 (d, J = 3.1 Hz, 1H; H-1), 5.22 (t, J = 10.2 Hz, 1H; H-3), 4.95 (t, J = 9.5 Hz, 1H; H-4), 4.33–4.01 (m, 7H; H-2, H-5, H-6, CH_{2Fmoc}, CH_{Fmoc}), 3.84–3.75 (m, 1H; CH^{α}), 3.13–3.05 (m, 2H; CH_2^{γ}), 1.99 (s, 3H; O(CO)*C*H_3), 1.96 (s, 3H; O(CO)*C*H_3), 1.92 (m, 4H, O(CO)*C*H_3; $CH^{\beta 1}$), 1.81 (s, 3H; O(CO)*C*H_3), 1.79–1.73 ppm (m, 1H; $CH^{\beta 2}$); ^{13}C NMR (101 MHz, $[D_6]$DMSO): δ = 170.5, 170.2, 169.7 (O(*C*O)CH_3), 156.0, 154.4, 144.4, 144.3 (COOH, CONH), 141.2, 128.1, 127.6, 125.7, 125.7, 120.6 (C^{Ar}), 90.8 (C-1), 70.6 (C-3), 69.1 (C-4), 69.0, 68.9, 65.9, 62.0, 53.8, 50.6, 49.1, 47.2 (CH_2^{Fmoc}, CH^{Fmoc}, C-2, C-5, C-6, C^{α}), 38.3 (C^{γ}), 32.7 (C^{β}), 22.7, 20.9, 20.9, 20.8 ppm, ((CO)*C*H_3); HRMS: m/z calcd for $C_{34}H_{40}N_3O_{14}^+$: 714.2505 $[M+H]^+$, found: 714.2498.

(2*R*)-2-((9-Fluorenylmethoxycarbonyl)amino)-4-(((2,3,4,6-tetra-*O*-acetyl-α-D-mannopyranosyl)-oxycarbonyl)amino)-butanoic acid (17): Compound **17** was prepared as described for compound **16** using Fmoc-D-Dab-OH **15** (1.15 g, 3.4 mmol), active carbonate **14** (1.91 g, 3.7 mmol) and diisopropylamine (1.3 mL, 7.4 mmol). The crude material was purified by FC (DCM/MeOH, 15:1 to 10:1) to give **17** as a white amorphous solid (2 g, 80%). $R_f = 0.40$(MeCN/H_2O 10:1); ^1H NMR (400 MHz, $[D_6]$DMSO): δ = 7.88 (d, J = 7.5 Hz, 2H; CH^{Ar}), 7.76 (m, 1H, NH^{γ}), 7.70 (d, J = 7.3 Hz, 2H; CH^{Ar}), 7.41 (t, J = 7.3 Hz, 2H, CH^{Ar}), 7.32 (t, J = 7.2 Hz, 1H; CH^{Ar}), 6.98 (m, 1H, NH^{α}), 5.86 (d, J = 1.7 Hz, 1H; H-1), 5.25 (dd, J = 10.1, 3.3 Hz, 1H; H-3), 5.19–5.14 (m, 1H; H-4), 5.10 (m, 1H; H-2), 4.30–4.01 (m, 6H; H-5, H-6ab, CH_2^{Fmoc}, CH^{Fmoc}), 3.82 (d, J = 5.4 Hz, 1H; CH^{α}), 3.17–3.01 (m, 2H; CH^{γ}), 2.12 (s, 3H; O(CO)*C*H_3), 2.01 (s, 3H; O(CO)*C*H_3), 1.99 (s, 3H; O(CO)*C*H_3), 1.95 (s, 3H; O(CO)*C*H_3), 1.93 (m, 1H; $CH^{\beta 1}$), 1.75 ppm (m, 1H; $CH^{\beta 2}$); ^{13}C NMR (101 MHz, $[D_6]$DMSO): δ = 170.4, 170.1, 169.8 (O(*C*O)CH_3), 144.4, 141.2 ((CO)NH), COOH), 126.1, 127.5, 125.7, 120.6 (CH_{Ar}), 90.4 (C-1), 69.8 (C-5), 68.9 (C-2), 68.7 (C-3), 65.9 (C-4), 65.6 (CH_{2-Fmoc}), 62.1 (C-6), 53.6 (C^{α}), 47.20 (CH^{Fmoc}), 38.3 (C_{γ}), 32.5 (C_{β}), 21.0 (O(CO)*C*H_3), 20.9 ppm (O(CO)*C*H_3); HRMS: m/z calcd for $C_{34}H_{39}N_2O_{15}^+$: 715.2345 $[M+H]^+$, found: 715.2347.

Peptide synthesis: Synthesis of peptides **1**–**10** was performed manually on NovaSyn TentaGel Sieber resin (Merck Millipore, resin loading 0.2 mmol g^{-1}) in 0.2 mmol scale for cyclic peptides and on Fmoc-Sieber-polystyrene resin (Iris Biotech, resin loading 0.61 mmol g^{-1}) in a 0.4 mmol scale for linear peptides. The resin was weighed into a disposable syringe equipped with a filter. Then, the resin was swollen in DMF (10 min), shaken with a solution of 20% (v/v) piperidine in DMF (1×3 min, 1×10 min) for Fmoc deprotection and washed with DMF (8×1 min) and NMP (2×1 min). Then, the coupling solution containing Fmoc-Xaa-OH (4 equiv), HBTU (3.8 equiv), HOBT (6 equiv) and EtN*i*Pr_2(8 equiv) in NMP (in case of glyco-D-Dab amino acids **16** and **17** all equivalents were divided by 2) was added. The coupling was performed for 1 h and monitored by Kaiser test.[33] In case of positive Kaiser test the reagents were refreshed otherwise the resin was washed with DMF (10×1 min) and the next coupling cycle was started. For peptides **1**, **2**, **4**, and **5** in the last coupling step a Boc-protected amino acid was used. For peptides **3** and **6**–**10** the last amino acid was Fmoc-protected. After the last coupling cycle the Fmoc group was removed as described above and the terminal amino group was acetylated by treatment with 10% (v/v) acetic anhydride in DMF (2× 15 min). Then the resin was washed with DMF (10×1 min) and CH_2Cl_2 (5×1 min) and dried for storage under reduced pressure. For the release of the peptide the resin was swollen in CH_2Cl_2

© 2016 Wiley-VCH Verlag GmbH & Co. KGaA, Weinheim

(10 min), washed with CH_2Cl_2 (3×1 min), and subsequently treated with TFA/triisopropylsilane/CH_2Cl_2 [1:1:98 (1×10 min, 3×2 min)], TFA/triisopropylsilane/Mix (Mix: CH_2Cl_2/trifluoroethanol 3:1) [1:1:98 (1×5 min, 2×2 min)], trifluoroethanol (2×2 min), CH_2Cl_2/trifluoroethanol [3:1 (2×2 min)], CH_2Cl_2 (2×2 min), methanol (2×2 min) and CH_2Cl_2 (2×2 min). All solutions were collected into a 10% (v/v) solution of pyridine in methanol. Then the solvent was evaporated. The residue was dissolved in a mixture of MeOH/$EtNMe_2$ 5:1 for deacetylation of the carbohydrate residues and stirred at room temperature until full conversion was reached according to LC/MS. The solvent was evaporated and the crude product was purified by semi-preparative HPLC.

Cyclopeptides 1 and 4: The peptide synthesis was performed as described above. After the last coupling step the resin was swollen in CH_2Cl_2 (10 min), treated with a solution of 1.6 equiv $Pd(PPh_3)_4$ and 30 equiv $BH_3{\cdot}NHMe_2$ in dry CH_2Cl_2 (2×30 min) for removal of Aloc and allyl protecting groups and washed with DMF (5×1 min) and with a solution of 0.5% (w/w) sodium diethyldithiocarbamate in DMF (10×1 min). Then the resin was treated with a solution of 5% (w/w) HOBT in DMF (10 min), washed with DMF (5×1 min), with NMP (2×1 min) and treated with a solution of HBTU (4 equiv), HOBT (6 equiv) and Et*N*iPr_2(8 eq) in NMP until the cyclization was complete according to LC-MS of a sample released from the resin. In case of incomplete cyclization the solution was refreshed. After completion, the resin was washed with DMF (6×1 min) and CH_2Cl_2 (5×1 min) and the resin was dried under reduced pressure. Release and deprotection of the peptide was performed as described above.

Glycopeptide 1: Purification by semi-preparative HPLC (Phenomenex Kinetex, 5–30% (B) in (A)+0.1% formic acid in 30 min). Analytical HPLC: t_R=18.7 min (Macherey–Nagel Nucleodur, 5–30% (B) in (A)+0.1% formic acid in 20 min); HRMS (ESI): calcd for $C_{81}H_{136}N_{19}O_{40}^+$: 2014.9186 $[M+H]^+$, found: 2014.9204.

Glycopeptide 2: Purification by semi-preparative HPLC (Phenomenex Gemini, 5–28% (B) in (A)+0.1% trifluoroacetic acid in 17 min). Analytical HPLC: t_R=18.8 min (Macherey–Nagel Nucleodur, 5–30% (B) in (A)+0.1% formic acid in 20 min); HRMS (ESI): calcd for $C_{76}H_{129}N_{18}O_{39}^+$: 1917.8659 $[M+H]^+$, found: 1917.8701.

Glycopeptide 3: Purification by semi-preparative HPLC (Phenomenex Gemini, 5–25% (B) in (A)+0.1% trifluoroacetic acid in 30 min). Analytical HPLC: t_R=15.8 min (Macherey–Nagel Nucleodur, 5–20% (B) in (A)+0.1% formic acid in 20 min); HRMS (ESI): calcd for $C_{64}H_{107}N_{15}O_{35}Na^+$: 1668.6946 $[M+Na]^+$, found: 1668.6968.

Glycopeptide 4: Purification by semi-preparative HPLC (Phenomenex Kinetex, 5–30% (B) in (A)+0.1% formic acid in 40 min). Analytical HPLC: t_R=18.7 min (Macherey–Nagel Nucleodur, 5–30% (B) in (A)+0.1% formic acid in 20 min); HRMS (ESI): calcd for $C_{77}H_{130}N_{17}O_{40}^+$: 1932.8655 $[M+H]^+$, found: 1932.8691.

Glycopeptide 5: Purification by semi-preparative HPLC (Phenomenex Gemini, 5–30% (B) in (A)+0.1% trifluoroacetic acid in 20 min). Analytical HPLC: t_R=18.6 min (Macherey–Nagel Nucleodur, 5–30% (B) in (A)+0.1% formic acid in 20 min); HRMS (ESI): calcd for $C_{72}H_{122}N_{16}O_{39}Na^+$: 1857.7947 $[M+Na]^+$, found: 1857.7977.

Glycopeptide 6: Purification by semi-preparative HPLC (Phenomenex Gemini, 5–25% (B) in (A)+0.1% trifluoroacetic acid in 20 min). Analytical HPLC: t_R=14.9 min (Macherey–Nagel Nucleodur, 5–20% (B) in (A)+0.1% formic acid in 20 min); HRMS (ESI): calcd for $C_{60}H_{101}N_{13}O_{36}Na^+$: 1586.6415 $[M+Na]^+$, found: 1586.6415.

Glycopeptide 7: Purification by semi-preparative HPLC (Knauer Eurospher, 5% isocratic (B) in (A)+0.1% formic acid in 10 min). Analytical HPLC: t_R=4.1 min (Macherey–Nagel Nucleodur, 5–10% (B) in (A)+0.1% formic acid in 20 min); MS (ESI): calcd for $C_{28}H_{48}N_7O_{17}^+$: 754.31 $[M+H]^+$, found: 754.25.

Glycopeptide 8: Purification by semi-preparative HPLC (Phenomenex Kinetex, 1–20% (B) in (A)+0.1% formic acid in 15 min). Analytical HPLC: t_R=10.7 min (Macherey–Nagel Nucleodur, 5–20% (B) in (A)+0.1% formic acid in 20 min); HRMS (ESI): calcd for $C_{33}H_{56}N_8O_{18}^+$: 852.3707 $[M]^+$, found: 852.3755 (deconvoluted).

Glycopeptide 9: Purification by semi-preparative HPLC (Phenomenex Kinetex, 1–20% (B) in (A)+0.1% formic acid in 20 min). Analytical HPLC: t_R=12.6 min (Macherey–Nagel Nucleodur, 5–30% (B) in (A)+0.1% formic acid in 20 min); HRMS (ESI): calcd for $C_{60}H_{101}N_{13}O_{35}^+$: 1563.6518 $[M]^+$, found: 1563.6621 (deconvoluted).

Glycopeptide 10: Purification by semi-preparative HPLC (Phenomenex Kinetex, 1–25% (B) in (A)+0.1% formic acid in 16 min). Analytical HPLC: t_R=12.5 min (Macherey–Nagel Nucleodur, 5–30% (B) in (A)+0.1% formic acid in 20 min); HRMS (ESI) calcd for $C_{60}H_{101}N_{13}O_{35}^+$: 1563.6518 $[M]^+$, found: 1563.6539 (deconvoluted).

Isothermal titration calorimetry: Isothermal titration calorimetry was performed on a GE Microcal iTC_{200} system. Wheat germ agglutinin was dissolved in buffer (50 mM sodium phosphate/50 mM KCl, pH 7.0), allowed to dissolve for 15 min and centrifuged for 5 min at 10,000 rpm. The protein concentration of the supernatant was determined by measuring the absorption at 280 nm using a theoretical extinction coefficient of 59200 $L\,mol^{-1}\,cm^{-1}$ (ExPASy ProtParam tool). The protein solution was diluted to a concentration of 20 μM for divalent ligands and 4 μM for tetravalent ligands. The ligands were dissolved in the same buffer solution and the concentration was adjusted to 20 fold of the protein concentration for divalent ligands and 10 fold for tetravalent ligands. The titrations were performed at 25 °C, 1000 rpm stirring speed, a reference power of 6 $\mu cal\,s^{-1}$ and an initial delay of 600 s for equilibration. Usually, 19 injections of 2 μL and duration of 4 s each were performed. Spacing between injections was 120 s. Prior to the first titration an injection of 0.4 μL was performed. The data were processed and analyzed using Origin 7 with the iTC Data analysis plugin by Microcal. Baseline correction and integration were carried out manually, and for data fitting the "one set of sites" model was used.

Dynamic light scattering: Dynamic light scattering was performed on a Viscotek 802 DLS system. WGA was dissolved in buffer (50 mM sodium phosphate/50 mM KCl, pH 7.0) and the protein concentration was determined as described above. Ligand concentrations were equal to the protein concentration for tetravalent ligands and twice the protein concentration for divalent ligands and are given in the Supporting Information. The solutions were filtered through a 100 nm cutoff filter (Whatman, Anotop 10, 0.1 μm, 10 mm) prior to measurement. The measurement was performed at 20 °C in a 12 μL sample cell, laser wavelength 830 nm, scattering angle 90°. Each sample was measured in duplicate with 10 scans over 5 s for each run. Evaluation of data was performed with OmniSIZE Version 3 by Viscotek.

Enzyme linked lectin assay: Assays were carried out as previously described[20a] using a different linker for coating of the microtiter plates. Briefly, microtiter plates with covalently immobilized reference ligand 11-amino-3,6,9-trioxaundecyl 2-acetamido-2-deoxy-β-D-glucopyranoside[34] were incubated with mixtures of horseradish peroxidase (HRP)-labeled WGA (1 $\mu g\,mL^{-1}$) and the respective WGA ligand in varying concentrations. After incubation, the plates were washed and remaining labeled WGA bound to the reference ligand was quantified by an HRP-catalyzed color reaction using 2,2′-azinobis(3-ethylbenzothiazoline-6-sulfonic acid) diammonium salt (ABTS) as substrate. From dose-response curves for inhibition of the bind-

© 2016 Wiley-VCH Verlag GmbH & Co. KGaA, Weinheim

ing of HRP-labeled WGA to the immobilized reference ligand, the concentrations that reduce the binding of labeled WGA by 50% (IC_{50} values) were determined as a measure of potency of the synthesized inhibitors.

Acknowledgements

This work was supported by the University of Konstanz and the Konstanz Research School Chemical Biology (KoRS-CB). P.R. acknowledges a PhD fellowship from KoRS-CB.

Keywords: isothermal titration calorimetry · lectins · multivalency · neoglycopeptides

[1] a) M. Mammen, S.-K. Choi, G. M. Whitesides, *Angew. Chem. Int. Ed.* **1998**, *37*, 2754 – 2794; *Angew. Chem.* **1998**, *110*, 2908 – 2953; b) C. Fasting, C. A. Schalley, M. Weber, O. Seitz, S. Hecht, B. Koksch, J. Dernedde, C. Graf, E.-W. Knapp, R. Haag, *Angew. Chem. Int. Ed.* **2012**, *51*, 10472 – 10498; *Angew. Chem.* **2012**, *124*, 10622 – 10650.

[2] a) G. Ercolani, L. Schiaffino, *Angew. Chem. Int. Ed.* **2011**, *50*, 1762 – 1768; *Angew. Chem.* **2011**, *123*, 1800 – 1807; b) C. A. Hunter, H. L. Anderson, *Angew. Chem. Int. Ed.* **2009**, *48*, 7488 – 7499; *Angew. Chem.* **2009**, *121*, 7624 – 7636.

[3] a) L. L. Kiessling, J. C. Grim, *Chem. Soc. Rev.* **2013**, *42*, 4476 – 4491; b) T. K. Dam, C. F. Brewer, *Adv. Carbohydr. Chem. Biochem.* **2010**, *63*, 139 – 164; c) R. J. Pieters, *Org. Biomol. Chem.* **2009**, *7*, 2013 – 2025; d) N. Jayaraman, *Chem. Soc. Rev.* **2009**, *38*, 3463 – 3483; e) A. Imberty, A. Varrot, *Curr. Opin. Struct. Biol.* **2008**, *18*, 567 – 576; f) B. E. Collins, J. C. Paulson, *Curr. Opin. Chem. Biol.* **2004**, *8*, 617 – 625; g) R. T. Lee, Y. C. Lee, *Glycoconjugate J.* **2000**, *17*, 543 – 551.

[4] a) H. Lis, N. Sharon, *Chem. Rev.* **1998**, *98*, 637 – 674; b) H.-J. Gabius, *Eur. J. Biochem.* **1997**, *243*, 543 – 576.

[5] a) Y. C. Lee, R. T. Lee, *Acc. Chem. Res.* **1995**, *28*, 321 – 327; b) J. J. Lundquist, E. J. Toone, *Chem. Rev.* **2002**, *102*, 555 – 578.

[6] a) Y. M. Chabre, R. Roy, *Adv. Carbohydr. Chem. Biochem.* **2010**, *63*, 165 – 393; b) O. Renaudet, R. Roy, *Chem. Soc. Rev.* **2013**, *42*, 4515 – 4517.

[7] a) M. Fiore, N. Berthet, A. Marra, E. Gillon, P. Dumy, A. Dondoni, A. Imberty, O. Renaudet, *Org. Biomol. Chem.* **2013**, *11*, 7113 – 7122; b) S. Cecioni, J.-P. Praly, S. E. Matthews, M. Wimmerová, A. Imberty, S. Vidal, *Chem. Eur. J.* **2012**, *18*, 6250 – 6263; c) F. Pertici, N. de Mol, J. Kemmink, R. J. Pieters, *Chem. Eur. J.* **2013**, *19*, 16923 – 16927.

[8] V. Wittmann, R. J. Pieters, *Chem. Soc. Rev.* **2013**, *42*, 4492 – 4503.

[9] a) V. Wittmann, *Curr. Opin. Chem. Biol.* **2013**, *17*, 982 – 989 and references therein; b) R. Visini, X. Jin, M. Bergmann, G. Michaud, F. Pertici, O. Fu, A. Pukin, T. R. Branson, D. M. E. Thies-Weesie, J. Kemmink, E. Gillon, A. Imberty, A. Stocker, T. Darbre, R. J. Pieters, J.-L. Reymond, *Acs Chem. Biol.* **2015**, *10*, 2455 – 2462.

[10] a) T. K. Dam, C. F. Brewer, *Biochemistry* **2008**, *47*, 8470 – 8476; b) D. Deniaud, K. Julienne, S. G. Gouin, *Org. Biomol. Chem.* **2011**, *9*, 966 – 979; c) M. Weber, A. Bujotzek, R. Haag, *J. Chem. Phys.* **2012**, *137*, 054111.

[11] a) P. Compain, A. Bodlenner, *ChemBioChem* **2014**, *15*, 1239 – 1251; b) S. G. Gouin, *Chem. Eur. J.* **2014**, *20*, 11616 – 11628.

[12] a) V. Wittmann, S. Seeberger, *Angew. Chem. Int. Ed.* **2000**, *39*, 4348 – 4352; *Angew. Chem.* **2000**, *112*, 4508 – 4512; b) V. Wittmann, S. Seeberger, *Angew. Chem. Int. Ed.* **2004**, *43*, 900 – 903; *Angew. Chem.* **2004**, *116*, 918 – 921; c) J.-L. Reymond, M. Bergmann, T. Darbre, *Chem. Soc. Rev.* **2013**, *42*, 4814 – 4822; d) A. Novoa, T. Eierhoff, J. Topin, A. Varrot, S. Barluenga, A. Imberty, W. Roemer, N. Winssinger, *Angew. Chem. Int. Ed.* **2014**, *53*, 8885 – 8889; *Angew. Chem.* **2014**, *126*, 9031 – 9035; e) S. Horiya, J. K. Bailey, J. S. Temme, Y. V. Guillen Schlippe, I. J. Krauss, *J. Am. Chem. Soc.* **2014**, *136*, 5407 – 5415; f) S. Ulrich, P. Dumy, *Chem. Commun.* **2014**, *50*, 5810 – 5825; g) M. L. Lepage, J. P. Schneider, A. Bodlenner, P. Compain, *J. Org. Chem.* **2015**, *80*, 10719 – 10733; h) C. S. Mahon, M. A. Fascione, C. Sakonsinsiri, T. E. McAllister, W. Bruce Turnbull, D. A. Fulton, *Org. Biomol. Chem.* **2015**, *13*, 2756 – 2761.

[13] a) C. S. Wright, *J. Mol. Biol.* **1980**, *141*, 267 – 291; b) C. S. Wright, *J. Mol. Biol.* **1989**, *209*, 475 – 487; c) K. Harata, H. Nagahora, Y. Jigami, *Acta Crystallogr. Sect. A* **1995**, *51*, 1013 – 1019.

[14] a) C. S. Wright, *J. Mol. Biol.* **1984**, *178*, 91 – 104; b) M. Muraki, M. Ishimura, K. Harata, *Biochim. Biophys. Acta Gen. Subj.* **2002**, *1569*, 10 – 20; c) C. S. Wright, G. E. Kellogg, *Protein Sci.* **1996**, *5*, 1466 – 1476.

[15] S.-I. Nishimura, T. Furuike, K. Matsuoka, K. Maruyama, K. Nagata, K. Kurita, N. Nishi, S. Tokura, *Macromolecules* **1994**, *27*, 4876 – 4880.

[16] a) D. Zanini, R. Roy, *Bioconjugate Chem.* **1997**, *8*, 187 – 192; b) A. Yamada, K. Hatano, T. Koyama, K. Matsuoka, N. Takahashi, K. I. P. J. Hidari, T. Suzuki, Y. Suzuki, D. Terunuma, *Bioorg. Med. Chem.* **2007**, *15*, 1606 – 1614; c) N. Parera Pera, H. M. Branderhorst, R. Kooij, C. Maierhofer, M. van der Kaaden, R. M. J. Liskamp, V. Wittmann, R. Ruijtenbeek, R. J. Pieters, *ChemBioChem* **2010**, *11*, 1896 – 1904; d) M. Ghirardello, K. Öberg, S. Staderini, O. Renaudet, N. Berthet, P. Dumy, Y. Hed, A. Marra, M. Malkoch, A. Dondoni, *J. Polym. Sci. Part A J. Polym. Sci. Part A: Polym. Chem.* **2014**, *52*, 2422 – 2433.

[17] T. Furuike, S. Aiba, S.-I. Nishimura, *Tetrahedron* **2000**, *56*, 9909 – 9915.

[18] A. Robinson, J.-M. Fang, P.-T. Chou, K.-W. Liao, R.-M. Chu, S.-J. Lee, *ChemBioChem* **2005**, *6*, 1899 – 1905.

[19] G. M. L. Consoli, F. Cunsolo, C. Geraci, V. Sgarlata, *Org. Lett.* **2004**, *6*, 4163 – 4166.

[20] a) C. Maierhofer, K. Rohmer, V. Wittmann, *Bioorg. Med. Chem.* **2007**, *15*, 7661 – 7676; b) R. Masaka, M. Ogata, Y. Misawa, M. Yano, C. Hashimoto, T. Murata, H. Kawagishi, T. Usui, *Bioorg. Med. Chem.* **2010**, *18*, 621 – 629; c) P. Braun, B. Nägele, V. Wittmann, M. Drescher, *Angew. Chem. Int. Ed.* **2011**, *50*, 8428 – 8431; *Angew. Chem.* **2011**, *123*, 8579 – 8582; d) H. S. G. Beckmann, H. M. Möller, V. Wittmann, *Beilstein J. Org. Chem.* **2012**, *8*, 819 – 826; e) S. André, S. O'Sullivan, C. Koller, P. V. Murphy, H.-J. Gabius, *Org. Biomol. Chem.* **2015**, *13*, 4190 – 4203.

[21] a) M. Lo Conte, S. Staderini, A. Chambery, N. Berthet, P. Dumy, O. Renaudet, A. Marra, A. Dondoni, *Org. Biomol. Chem.* **2012**, *10*, 3269 – 3277; b) A. Marra, S. Staderini, N. Berthet, P. Dumy, O. Renaudet, A. Dondoni, *Eur. J. Org. Chem.* **2013**, 1144 – 1149.

[22] D. Schwefel, C. Maierhofer, J. G. Beck, S. Seeberger, K. Diederichs, H. M. Möller, W. Welte, V. Wittmann, *J. Am. Chem. Soc.* **2010**, *132*, 8704 – 8719.

[23] a) A. K. Allen, A. Neuberger, N. Sharon, *Biochem. J.* **1973**, *131*, 155 – 162; b) Y. Nagata, M. M. Burger, *J. Biol. Chem.* **1974**, *249*, 3116 – 3122; c) I. J. Goldstein, S. Hammarström, G. Sundblad, *Biochem. Biophys. Acta* **1975**, *405*, 53 – 61.

[24] T. Seitz, C. Maierhofer, D. Matzner, V. Wittmann, in *Carbohydrate Chemistry: Proven Synthetic Methods, Vol. 3* (Eds.: R. Roy, S. Vidal), CRC Press, Boca Raton, **2015**, pp. 215 – 218.

[25] M. M. Sim, H. Kondo, C. H. Wong, *J. Am. Chem. Soc.* **1993**, *115*, 2260 – 2267.

[26] P. Sieber, *Tetrahedron Lett.* **1987**, *28*, 2107 – 2110.

[27] R. Knorr, A. Trzeciak, W. Bannwarth, D. Gillessen, *Tetrahedron Lett.* **1989**, *30*, 1927 – 1930.

[28] T. K. Dam, C. F. Brewer, in *Lectins* (Ed.: L. N. Carol), Elsevier Science B. V., Amsterdam, **2007**, pp. 75 – 101.

[29] W. B. Turnbull, A. H. Daranas, *J. Am. Chem. Soc.* **2003**, *125*, 14859 – 14866.

[30] The molecular mass of the WGA dimer is 34 kDa indicating that the values calculated from the DLS experiments by OmniSIZE 3.0 with the built-in protein model overestimate the correct values. In spite of this deviation of absolute values, the formation of aggregates with increased size is clearly detected.

[31] C. Sisu, A. J. Baron, H. M. Branderhorst, S. D. Connell, C. A. G. M. Weijers, R. de Vries, E. D. Hayes, A. V. Pukin, M. Gilbert, R. J. Pieters, H. Zuilhof, G. M. Visser, W. B. Turnbull, *ChemBioChem* **2009**, *10*, 329 – 337.

[32] W. L. DeLano, The PyMOL Molecular Graphics System, DeLano Scientific LLC, San Carlos, CA, USA.

[33] E. Kaiser, R. L. Colescott, C. D. Bossinger, P. I. Cook, *Anal. Biochem.* **1970**, *34*, 595 – 598.

[34] A. E. Zemlyakov, V. O. Kur'yanov, E. A. Sidorova, T. A. Chupakina, V. Y. Chirva, *Chem. Nat. Compd.* **1998**, *34*, 563 – 567.

Received: February 11, 2016
Published online on ■■ ■■, 0000

© 2016 Wiley-VCH Verlag GmbH & Co. KGaA, Weinheim

FULL PAPER

Both cyclic and linear tetravalent glycopeptides bind with nanomolar affinity to the model lectin wheat germ agglutinin regardless of their backbone flexibility. Different binding modes of tetravalent and divalent ligands could be elucidated using isothermal titration calorimetry, enzyme linked lectin assays, and dynamic light scattering.

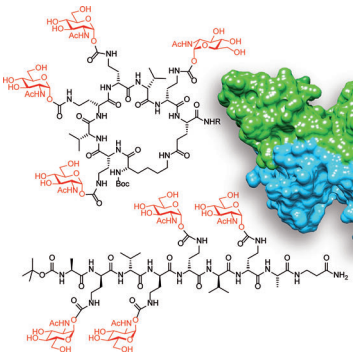

Neoglycopeptides

*P. Rohse, V. Wittmann**

■■ – ■■

Mechanistic Insight into Nanomolar Binding of Multivalent Neoglycopeptides to Wheat Germ Agglutinin

© 2016 Wiley-VCH Verlag GmbH & Co. KGaA, Weinheim